PCCP

Accepted Manuscript

ROYAL SOCIETY OF CHEMISTRY

www.rsc.org/pccp

Energy & Environmental Science RSCPublishing

ARTICLE

Efficiency limitations in a low band-gap Diketopyrrolopyrrole-based polymer solar cell

Cite this: DOI: 10.1039/x0xx00000x

Sebastian Albert-Seifried[a,*,§], Doo-Hyun Ko[a,c,§], Sven Hüttner[a], Catherine Kanimozhi[b], Satish Patil[b], Richard H. Friend[a]

Received 00th January 2012,
Accepted 00th January 2012

DOI: 10.1039/x0xx00000x

www.rsc.org/

We report the performance and photophysics of a low band-gap, high p-type mobility diketopyrrolopyrrole-based copolymer for used in bulk heterojunction devices in combination with $PC_{71}BM$. We show that the short lifetime of photogenerated excitons in the polymer constitutes an obstacle towards device efficiency by limiting the diffusion range of the exciton to the donor-acceptor heterojunction. We employ ultrafast transient-probe and fluorescence spectroscopy techniques to examine the excited state loss channels inside the devices. We use the high boiling point solvent additive 1,8-diiodooctane (DIO) to study the photoexcited state losses in different blend morphologies. The solvent additive acts as compatibiliser between the donor and acceptor material and leads to smaller domain sizes, higher charge formation yields and increased device efficiency.

Broader context

Organic solar cells have long been regarded as low-cost alternatives for silicon-based solar cells, but are suffering under low power conversion efficiencies. In order to increase device efficiencies, advances in the understanding of the materials and the loss mechanisms are essential. One of the major trends is the development of low band-gap polymers, which capture a larger part of the solar irradiation spectrum. However, few low band-gap material systems have achieved external quantum efficiencies higher than 60%. An important loss-channel is that of non-radiative decay losses during exciton diffusion to the interface. This loss mechanism is particularly strong for low band-gap polymer systems and therefore has wide-ranging ramifications for the trend towards even lower band-gap polymers. This investigation, which puts particular emphasis on analysing and quantifying the loss mechanisms in the devices, sets an example of how the morphological impact of solvent additives in organic solar cells can be examined and used to reduce these losses.

Introduction

Power conversion efficiencies of at least 10% are generally regarded as requirement for the commercialization of organic solar cells. This generally requires a low band-gap materials system and active layer thicknesses above 100 nm to capture a large part of the solar spectrum. The short exciton diffusion lengths in conjugated polymers of only 5-10 nm [1] has led to the development of bulk hetero-junctions.[2, 3] These intermixed donor-acceptor blends can be easily obtained by depositing a film from a solution containing both materials.

The right morphology roughness in these films is crucial to allow both efficient charge separation at the interface and efficient charge extraction from the device. Feature sizes larger than the exciton diffusion length will result in some excitons decaying to the ground state rather than reaching the BHJ interface, thus reducing the overall device efficiency. Inversely, too fine morphologies are detrimental to percolation pathways which are required for efficient charge carrier extraction from the device. The optimal morphology thus depends on the exciton diffusion length and the charge carrier mobility in each of the two materials as well as the overall film thickness. The exciton diffusion length for emissive materials can be obtained by measuring the exciton quenching for different polymer film thicknesses on an exciton scavenging substrate.[1, 4] Exciton diffusion in conjugated polymers takes place by two separate processes, short-range electron tunnelling processes and Förster type resonant energy transfer (FRET).[5, 6] The efficiency of both mechanisms depend on the singlet exciton lifetime. The singlet exciton lifetime is therefore an important parameter for the efficiency of OPV systems. While the trend towards low band-gap polymers allows the absorption of a wider solar radiation spectrum, lowering the band-gap also has the detrimental effect

Notes and References

a Cavendish Laboratory, Department of Physics, University of Cambridge, Cambridge, CB3 0HE, UK.
b Solid State and Structural Chemistry Unit, Indian Institute of Science, Bangalore 560012, India.
c Center for Opto-Electronic Convergence Systems, Korea Institute of Science and Technology, Seoul 136-791, South Korea
§ These authors contributed equally to the work.
† Electronic Supplementary Information (ESI) available: See DOI: 10.1039/b000000x/

of shorter exciton lifetimes. According to the energy gap law the non-radiative decay rate by multi-phonon processes increases exponentially with a reduction of the band-gap.[7-9] As an example case to demonstrate the implications of the energy gap law on the trend towards low band-gap polymers, we have chosen a diketopyrrolopyrrole-based (DPP) polymer blended with $PC_{71}BM$. The clear separation of the absorption spectra of the polymer PTDPPQz and the $PC_{71}BM$ allows us to selectively excite either the polymer or the $PC_{71}BM$ and to assess the excited state processes that occur after photoexcitation. In order to examine the extent to which morphology control can be used to overcome the shortfalls of a short exciton lifetime, we varied the domain sizes with the use of small amounts of high boiling point solvent additives. In recent years, the use of mixed solvent [10, 11] and high boiling point solvent additives [12] have emerged as a promising and versatile method to control the morphology during the spin-coating process. Generally, solvent additives are used with the purpose of coarsening the morphology,[10, 13-17] for example by pre-aggregating the material with the lower solubility. The solvent additive thus performs the same blend-coarsening role as thermal annealing. Some of the blends coarsened by this method have shown a reduction in the geminate recombination losses [13, 14] and an increased charge carrier mobility.[10, 14] The reduction in geminate recombination has been attributed to an 'interface modification' where a locally ordered interface between donor and acceptor is formed.[13] More recently, solvent additives have also been used to modify the BHJ in the opposite direction, towards a finer morphology.[18-21] The observation that the same solvent additive can lead to completely opposite effects shows the complexity of the system and the interplay between solubilities between fullerene derivatives, polymers and solvents. Therefore solvent additives are often used on a trial-and-error basis.

Results

Device Performance

We investigated the influence of the high boiling point solvent additive 1,8-diiodooctane (DIO) on a donor-acceptor system comprising $PC_{71}BM$ and the low band-gap diketopyrrolopyrrole-based (DPP) polymer shown in the inset of Figure 1 (b). DPP-based polymers have recently emerged as a promising new material class, and have achieved device efficiencies in the range of 6-7% PCE.[17, 22-24] In the material system studied here, the addition of small quantities (2.5 vol. %) of the solvent additive DIO to the main solvent led to remarkable increases in the device efficiency by more than a factor of three. A detailed description of the polymer synthesis can be found in the supplementary information. Standard solar cells with different polymer to $PC_{71}BM$ ratios and different active layer thicknesses were fabricated under nitrogen atmosphere. For both the devices made with and without solvent additive, the highest efficiencies were achieved using a 1:4 polymer:$PC_{71}BM$ ratio and an active layer thickness of approximately 80 nm. These films were achieved by spin-coating from a 12 mg/ml chlorobenzene solution at 1200 rpm. Higher polymer concentrations led to visibly inhomogeneous films due to the poor solubility of the polymer. For the devices with DIO, 2.5% by volume of the high boiling point solvent additive was added to the solution before spin-coating. The films were then left under approx. 10^{-5} mbar vacuum for at least one hour to remove the remaining solvent additive. The absorption spectra of the polymer, the $PC_{71}BM$ and the blends are shown in Figure 1 (a).

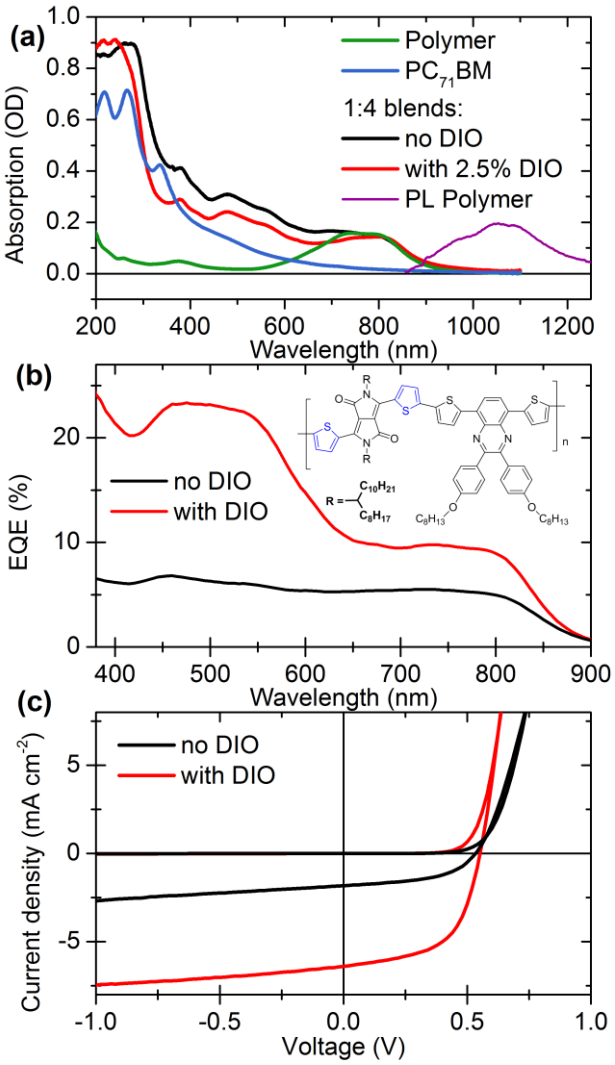

Figure 1: (a) Steady state absorption spectra of the polymer film, a $PC_{71}BM$ film and 1:4 polymer:$PC_{71}BM$ films prepared without and with the solvent additive DIO, as well as the polymer photoluminescence spectrum. The polymer absorption spectrum was rescaled for better comparison. (b,c) EQE spectra, JV- and dark current curves of the devices prepared with 2.5% solvent additive DIO and without additives. The inset of (b) shows the chemical structure the DPP-polymer.

For the devices, a 100 nm aluminium electrode was evaporated, after which they were characterized in a home-built PV testing rig under an AM 1.5 solar simulator. The external quantum efficiency (EQE) curves and the photocurrent curves are shown in Figure 1 (b) and (c). The devices made without and with the solvent additive DIO showed an average power conversion efficiency of 0.6% and 2.1% respectively, while the short-circuit current was increased from 2.2 to 6.6 $mAcm^{-2}$. We note that the strongest increase in the EQE curves where observed between 400 and 600 nm, the spectral region where mainly the $PC_{71}BM$ absorbs.

In the following sections, we investigate the effect of the DIO on the blend morphology, as well as the excited state dynamics and loss mechanisms in these devices. We use scanning electron microscopy (SEM) to examine changes in the morphology, photoluminescence (PL) quenching measurements to investigate which fraction of excited states reach the donor-

acceptor interface and broadband transient absorption to probe the overall evolution of the excited states population over time.

Photocurrent Contributions of Polymer and $PC_{71}BM$

The general understanding of OPV systems is based on the excitation of the polymer domains and the subsequent electron transfer from the "electron donor" polymer to the "electron acceptor" $PC_{71}BM$. The charge generation after excitation of the $PC_{71}BM$ domains is rarely considered as a major contribution to the device performance. In the system studied here, the devices with and without the solvent additive DIO both show a higher EQE for the $PC_{71}BM$ absorption region (Figure 1 b). Especially for the device prepared with DIO, the $PC_{71}BM$ absorption is the dominant feature in the EQE spectrum. In order to quantify the contributions to the photocurrent by absorption in the polymer and the $PC_{71}BM$ domains, the photocurrent spectra are examined as shown in Figure 2 (solid lines). These spectra were obtained by multiplying the solar irradiation spectrum (AM 1.5) in photon flux intensity with the external quantum efficiency spectrum. The dotted and dashed lines show the contributions of the $PC_{71}BM$ and polymer absorption to J_{SC} respectively. These spectra were obtained by comparison of the absorption spectra of $PC_{71}BM$, the polymer and the blends. In both devices the larger contribution to J_{SC} comes from the $PC_{71}BM$ absorption which accounts for 56% and 64% of the photocurrent generated for the devices prepared without and with DIO. We note that in the device prepared with DIO, almost 2/3 of the photocurrent is contributed by the $PC_{71}BM$ absorption.

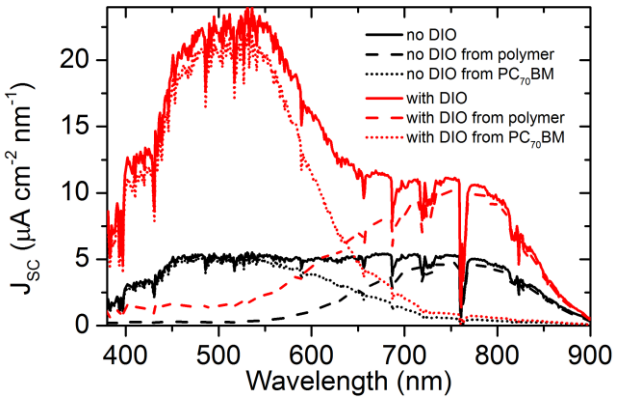

Figure 2: The solid lines show the spectral composition of the short-circuit current under solar illumination AM 1.5 for devices prepared with DIO (red lines) and without DIO (black line). The relative contribution by the $PC_{71}BM$ (dotted line) and polymer (dashed line) are also shown.

In order to probe if the stronger $PC_{71}BM$ contribution to the photocurrent is caused by phenomena before or after excitons are split at the donor-acceptor interface, we measured the voltage dependence of photocurrent generated in fullerene-derivative and in polymer phases. Work by Brenner et al. has suggested differences in the nature of fullerene exciton-produced and polymer exciton-produced interfacial electron-hole pairs for some polymer-PCBM systems.[25] Figure 3 a) shows the three different excitation spectra used to probe the photo response in different regions of the absorption spectra, i.e. to excite predominantly the $PC_{71}BM$, the polymer domains or both materials and the corresponding JV-curves are shown in Figure 3 b). The intensity of the three excitation spectra were adjusted by optical density filters in a way to obtain identical short-circuit currents for all three excitation spectra. The losses due to non-geminate recombination of charges will therefore be comparable for all three excitation spectra. The photocurrent curves were found to be almost identical for excitation of the $PC_{71}BM$ and the polymer. The identical bias-dependence under different excitation spectra indicates that the same charge pair states are created after exciting the polymer and the $PC_{71}BM$. This further suggests that the subsequent geminate recombination losses are the same for excitation of both materials (under the assumption that interfacial states are connected to the electrodes by conduction pathways).

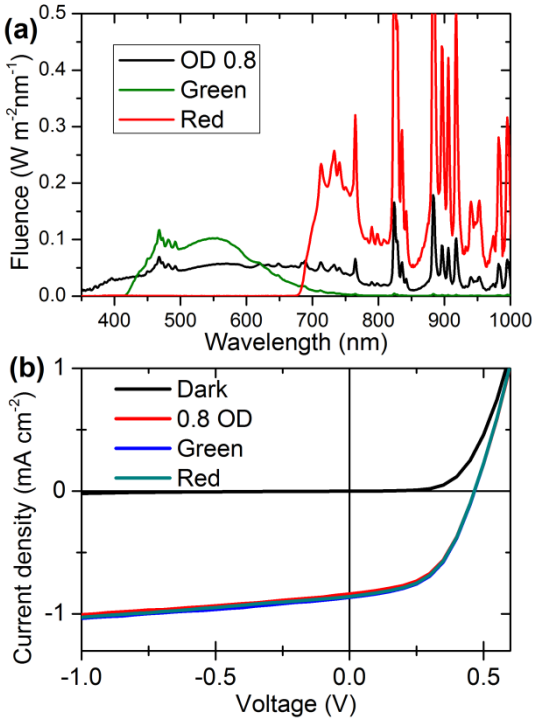

Figure 3: JV-curves under illumination in different spectral regions (with DIO). a) shows the different illumination spectra and (b) the corresponding JV-curves.

Morphological Investigation and Blend Formation

To directly visualize the effect of DIO on the morphology of the blend, we employed scanning electron microscopy (SEM) measurements. It is well documented that the contrast obtained by SEM between polymer:fullerene domains is very poor. To overcome this limitation, we selectively removed the $PC_{71}BM$ from the films before the measurements. The $PC_{71}BM$ was removed by a modified procedure following Friedel et al.,[26] and as described in the supplementary information. The SEM images of the blends prepared without and with DIO are shown in Figure 4 a) and b). The film prepared from a dichlorobenzene solution without solvent additives shows macro-scale phase separation resulting in domain sizes on the scale of ~100 nm, whereas a finely intermixed morphology was obtained for the blend prepared with 2.5% DIO in chlorobenzene.

The crystallinity of the DPP polymer is strongly affected by the addition of $PC_{71}BM$ which reduces the ordering in the polymer. As shown in X-ray studies in the supplementary information, the size and crystallinity of the polymer domains further decrease under the addition of DIO. By contrast, the crystallinity of the $PC_{71}BM$ domains tends to increase by processing with DIO. Similar findings have previously been attributed to the better solubility of $PC_{71}BM$ in DIO and the

improved aggregation of $PC_{71}BM$ after evaporation in this high boiling point solvent.[10, 19]

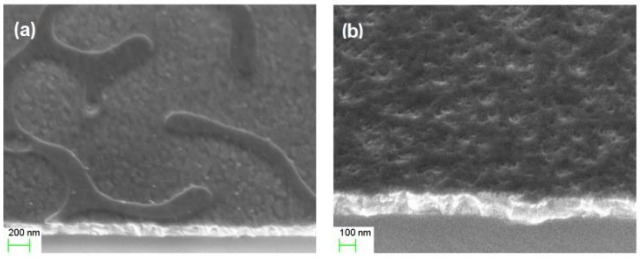

Figure 4: Scanning Electron Microscopy images of the polymer domains after selectively dissolution of the $PC_{71}BM$ part for films prepared (a) without (b) and with the solvent additive DIO.

In the majority of publications which investigate the role of solvent additives, the solvent additive is reported to enhance the solubility contrast between the two materials, therefore causing one of the materials to fall out of solution leading to coarser morphologies. We believe that in the system studied here, the solvent additive DIO rather acts as a compatibilizer i.e. common solvent between the two materials. Both the polymer and the $PC_{71}BM$ are soluble in chlorobenzene, though the polymer solubility is much lower with around 15mg/ml as compared to 110 mg/ml for $PC_{71}BM$.[27] The additive DIO is a good solvent for $PC_{71}BM$ and a residual amount of the solvent remains within the film after spin coating, leaving the polymer film in a swollen state and helping the $PC_{71}BM$ to finely intermix and percolate.

When only chlorobenzene is used as a single solvent, the blend behaves as an incompatible system and phase-separates on a macroscopic length-scale. The polymer and $PC_{71}BM$ form large domains as seen in Figure 4 a). The tendency to phase separate and the only low solid state solubility of $PC_{71}BM$ within the polymer has been confirmed in crystallisation experiments with different contents of $PC_{71}BM$ (see supporting information) where films were annealed for extended times towards their thermodynamic equilibrium.

The film formation process changes entirely when 2.5 volume % DIO is added to the solution. During spin-coating the chlorobenzene evaporates much faster (within seconds) compared to DIO (which can partialy remain in the film for several hours), therefore gradually increasing the volume fraction of DIO. After the majority solvent has evaporated, a binary, non-miscible system is left behind in which the polymer is no longer soluble but still swollen by the remaining DIO. The important role of the DIO, which is a good solvent for $PC_{71}BM$ is therefore to act as a compatibilizer distributing the $PC_{71}BM$ within the polymer. This ultimately leads to the formation of a much finer interdispersed morphology. Other crystalline polymer – fullerene systems such as P3HT:PCBM show that the length scale of phase separation is then determined by the intrinsic size of crystalline polymer lamellae leading to finely interdispersed network on the 10 nm scale.[28] A schematic of the proposed mechanism by which the solvent additive prevents a large scale phase separation is shown in the supplementary information. After spin-coating the DIO can finally be removed from the blend by placing the samples under vacuum for approximately 30 minutes.

Another high boiling point solvent additive which acts in the opposite way was 1,8-octanedithiol (ODT). When 5 volume % of ODT was added to the solution an even stronger phase separation occurred compared to the blend without solvent additives, leading to large domains which were clearly visible under a standard optical microscope (~1 µm).

In order to obtain further information regarding the purity of the domains as seen in the SEM images, photoluminescence (PL) quenching measurements were taken for both the polymer and $PC_{71}BM$. The results are shown in Figure 5. To measure the polymer PL quenching (solid symbol), the samples were excited using a 795 nm cw laser and the PL was detected using an integrating sphere and spectrometer. To account for different sample thicknesses, the difference in the laser absorption was factored in as described in literature.[29] The polymer photoluminescence quantum efficiency is very low. We measured this to be 0.06 (±0.03) % and was significantly quenched in the blends. With the addition of 50% (80%) of $PC_{71}BM$ by weight the PL intensity decreased by around 20% (30%) for the blends without DIO and by around 40% (50%) for the blends with DIO. As expected, the polymer PLQE decreases with increased $PC_{71}BM$ concentration and with the addition of DIO. We note that even with the 1:4 polymer:$PC_{71}BM$ ratio and solvent additive, only about 50% of the excited states seem to be quenched at the interface. We will discuss this in detail in the following section.

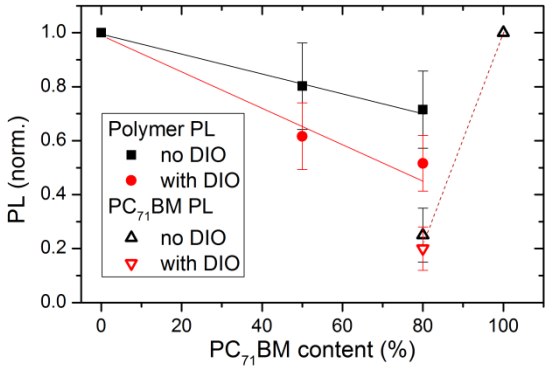

Figure 5: Photoluminescence efficiencies for the blends normalized to the PL intensities of the pure films. The solid symbols show the polymer PL after excitation under excitation at 790 nm and the open symbols show the $PC_{71}BM$ PL under excitation at 532 nm. For all measurements the PL was integrated over the entire emission spectra.

The $PC_{71}BM$ PL quenching measurements (open symbols) were taken under laser excitation at 470 nm where the polymer shows little absorption. We found that even for the very coarse blend prepared without solvent additive, the PL intensity decreased by 75% compared with the PL intensity of a $PC_{71}BM$ only film and after correction for the $PC_{71}BM$ absorption. As the $PC_{71}BM$ exciton diffusion length (~5-10 nm) [30] is much shorter than the ~100 nm domain sizes seen in the SEM images, these results strongly suggest polymer impurities in the $PC_{71}BM$ domains, which help to quenching the $PC_{71}BM$ excitons. In the films prepared with DIO an even larger part of around 80% of excitons is quenched.

Short-time TA with Excitation of Polymer

In order to study how the additives affect the excited states dynamics, broadband sub-picosecond transient absorption (TA) measurements were carried out using the setup described in literature [31] with the following further improvements: The detection system was replaced by a dual line camera with two

visible-near infrared photodiode arrays (Stresing Entwicklungsbüro, Hamamatsu G11608-512 PDAs) and a new homebuilt infrared noncollinear optical parametric amplifier as described in literature [32] was used to probe the near-infrared region at 1100-1600 nm. In TA measurements under medium-strong to strong excitation intensities, bimolecular recombination processes can create additional decay channels and lead to a faster decay. To avoid these well-known bimolecular decay processes, measurements were carried out in the linear excitation regime, where the excited state kinetics are independent of the excitation intensity whenever possible. The TA spectra in Figure 6 a) and c), as well as all short-time kinetics (Figure 7 and Figure 8) were found to be in the linear excitation regime. Bimolecular processes by exciton-exciton quenching and bimolecular charge recombination can therefore be ruled out in the interpretation of the results.

Figure 6 shows the broadband TA spectra of (a) a DPP-polymer film, (b) a $PC_{71}BM$ film and (c) a 1:4 polymer:$PC_{71}BM$ blend prepared without solvent additives. The spectra of the polymer film (a) after excitation at 800 nm with 2.5 μJcm^{-2} show a clear ground-state bleach (GSB) at 600-850 nm and a broad excitonic photoinduced absorption (PIA) above 850 nm. We note that the very narrow spectral features with widths less than 50 nm are caused by artefacts in the measurement and henceforth ignore them. As shown later, the polymer excitons are very short-lived with a lifetime of 35 ps and most of the signal has disappeared after 100 ps.

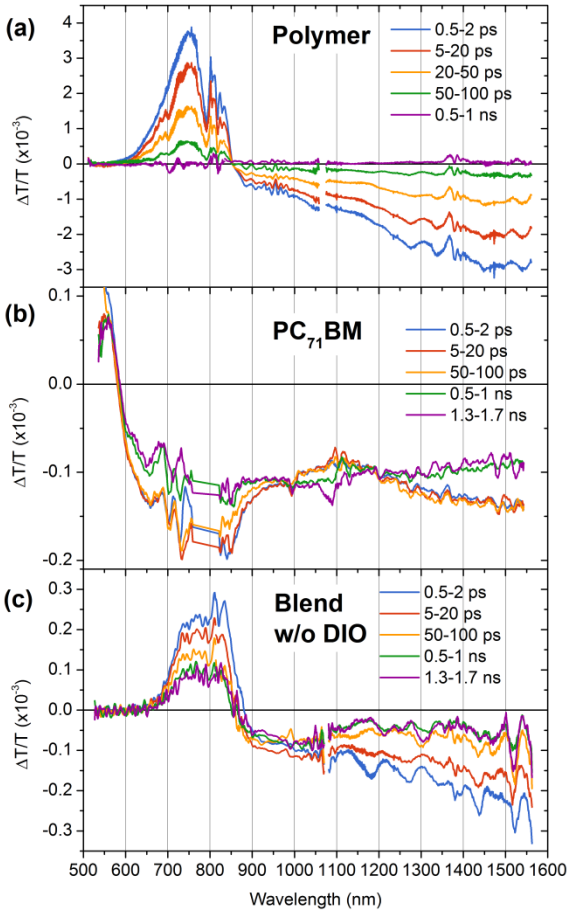

Figure 6: Broadband sub-picosecond TA spectra of (a) the DPP-polymer film excited at 800 nm, (b) a $PC_{71}BM$ film excited at 530 nm and (c) a 1:4 polymer-$PC_{71}BM$ blend prepared without solvent additive and excited at 800 nm. The excitation fluence was 2.5 μJcm^{-2} for (a), 6 μJcm^{-2} for (b) and 1-2 μJcm^{-2} for (c). TA spectra were measured in 3 consecutive measurements with broadband probe spectra ranging from approximately 500-800 nm, 800-1050 nm and 1100-1600 nm. In (c) the spectra were rescaled according to the slightly different excitation intensities in the different probe ranges.

The spectra of the $PC_{71}BM$ film shown in Figure 6 (b) after excitation at 530 nm with 6 μJcm^{-2} pulses show a faint GSB below 580 nm, followed by a broad PIA spectrum. Because of the much lower excited state cross-section of $PC_{71}BM$, the signal intensity was almost one order of magnitude weaker than that of the polymer film, despite higher excitation fluence. As a consequence of the weak signal strength the TA spectra are significantly noisier than that of the polymer film. Over the timescale of around 1 ns the TA spectrum flattens significantly, which has been attributed to the intersystem-crossing of singlet excitons to triplet states.[33]

The TA spectra of a 1:4 DPP-polymer:$PC_{71}BM$ blend prepared without DIO and excited at 800 nm are shown in Figure 6 **(c)**. The most prominent features in these spectra are the strong polymer GSB, centred at 800 nm and a broad PIA beyond 850 nm. Because of the excitation at 800 nm, where only the polymer absorbs, the initial TA spectrum (averaged between 0.5-2 ps) closely resembles the TA spectra of the pure polymer film (a) with a continuously sloped PIA band. At later delay times, the PIA band gradually broadens to a broad negative signal. The broad, flat PIA band is consistent with previous observations of charge formation in polymer-PCBM blends.[34] Over time, the GSB at 800 nm gradually recovers but does not shift spectrally. Both the polymer excitons and the charge pairs between the polymer and the $PC_{71}BM$ cause a GSB (positive signal) in this spectral region. Measuring the signal intensity at this wavelength therefore allows probing the combined population of polymer excitons and charge pairs over time. Figure 7 shows the normalized TA kinetics of the GSB (averaged over 750-830 nm) of the polymer only film and of different 1:4 polymer:$PC_{71}BM$ blends after excitation at 800 nm.

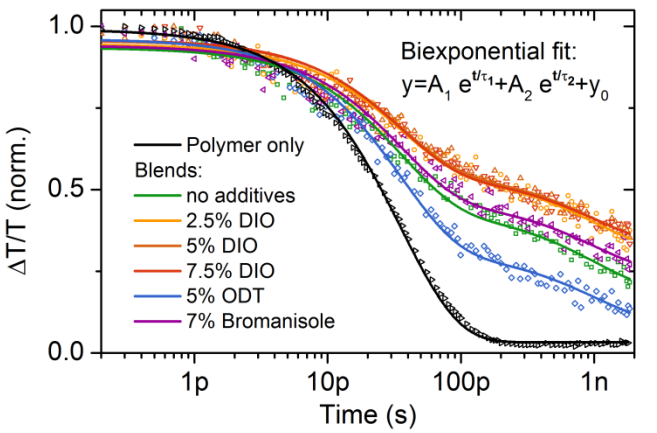

Figure 7: Transient Absorption kinetics of the polymer GSB (averaged over 750-820 nm) for the polymer only film and for blends with $PC_{71}BM$. Excitation wavelength was 800 nm.

The fastest decay can be observed for the polymer-only film, which decays to about 3% within 200 ps and remains flat thereafter. These 3% long-lived flat signals are caused by a temperature-induced artefact, which is common, but rarely identified in TA measurements in the GSB region.[35] In the first 200 ps the decay of the polymer-only film follows an almost perfect mono-exponential decay with a 35 ps time constant.

Table 1 : Parameters for the bi-exponential fit of the TA kinetics shown in Figure 7.

	A1	t1 (ps)	A2	t2 (ps)	y0
no additives	53%	35	27%	1000	20%
2.5% DIO	43%	35	24%	1000	33%
5% DIO	42%	35	24%	1000	34%
7.5% DIO	43%	35	22%	1000	35%
5% ODT	68%	35	23%	1000	9%
7% Bromoanisole	50%	35	23%	1000	27%
polymer only	96%	35.3	-	-	3%

The polymer-$PC_{71}BM$ blends all show much slower decay kinetics and follow a clear trend towards slower decays for finer morphologies. Besides blends with various amounts of DIO, the figure also shows kinetics of blends prepared with the solvent additives Bromoanisole and ODT. The blend prepared with ODT shows large-scale phase separation which exceeds those of the blends without additives and shows the fastest decay kinetics of all blends. All the kinetics can be well fitted with a double exponential decay, where the time constant of the first component is set to the polymer exciton lifetime of 35 ps. The fitting parameters are shown in Table 1. The first decay component, with stronger amplitude in the coarse blends therefore represents the polymer excitons which decay back to the ground state before reaching the polymer:$PC_{71}BM$ interface. As expected, the films processed with the solvent additive DIO, which showed the finest morphology, exhibit the weakest fast decay component. However, the amount of DIO added does not have any effect on the decay kinetics. As all polymer excitons decay with a 35 ps lifetime within 200 ps, we assign the remaining signal thereafter to interfacial charge-transfer (CT) states and free charges.[36] We note that all the blend kinetics show a further strong decay between 200 ps and 2 ns. As these measurements were carried out in the linear excitation regime, bimolecular charge recombination can be ruled out and the second exponential decay component is assigned to geminate recombination of CT-states.

In the coarsest blend, prepared with 5% ODT, almost 70% of excitons decay before reaching the heterojunction within the first 200 ps. This fraction drops to around 50% for the blend prepared without additive and around 40% with DIO, with again, no significant variations with the amount of DIO added. The high fraction of excitons which decay with the polymer exciton lifetime corresponds well with the values observed from the polymer quenching measurements. In the same order, the amount of long-lived charges (>2 ns) increases from around 10% to 20% and 35%. The amount of CT-states which recombine geminately within 2 ns remains relatively unchanged at about 25%.

However, when only the excited states which reach the donor-acceptor interface are considered, the ratio of free charges to CT-states increases significantly in the blends with DIO. This suggests that excitons have a higher chance of forming free charges which can be extracted from the device implying a finer and more defined morphology.

A comparison between the domain sizes in the SEM images (Figure 4) and the exciton diffusion length suggests that not all polymer excitons are quenched at interfaces between two pure domains. The size of the polymer domains in the blend prepared without additive is around 100 nm and far exceeds the ~5 nm exciton diffusion length for the polymer. This implies that a large fraction of the ~50% excitons are quenched at defect sites, such as isolated $PC_{71}BM$ molecules within the polymer domains. Excitons diffusing to these isolated $PC_{71}BM$ molecules can be dissociated but as the electrons cannot escape from the interface fast geminate recombination occurs. In the coarsest blends (with 5% ODT), over two thirds of the longer-lived (>200 ps) excited states recombine geminately.

Holcombe *et al.* have shown that the local morphology at the interface is an important parameter in the charge separation efficiency,[37] and both ODT [13] and DIO [14] have been observed to reduce geminate recombination in systems where they lead to coarser morphologies. The data presented here suggest that the changes in geminate recombination can also be explained by an increased ratio of excitons which are quenched between two pure domains and those quenched at isolated $PC_{71}BM$ molecules for the improved morphology obtained with DIO. The most significant improvement in device performance of the solvent additive therefore originates from the increased charge formation yield rather than from a reduction of geminate recombination. We also note that the amount of long-lived excited states correspond well with the ~30-35% internal quantum efficiency of the blends without additives and with 2.5% DIO at 800 nm.

Short-time TA with $PC_{71}BM$ Excitation

In order to also probe the hole transfer from the $PC_{71}BM$ domains to the polymer, further broadband TA measurements were taken with excitation at λ=530 nm. As illustrated in Figure 1 (a), this wavelength mainly excites the $PC_{71}BM$ domains (~90%) and only a small fraction (8-10%) of the initial excitation is created inside the polymer domains. Figure 8 a) shows the kinetics averaged over 750-820 nm, a region where the polymer GSB overlaps with the $PC_{71}BM$ PIA. As mentioned previously, the polymer excited state cross-section is around 30 times stronger than that of the $PC_{71}BM$, causing the $PC_{71}BM$ PIA (negative signal) to be hidden behind the stronger polymer GSB (positive signal). Consequently, the kinetics are convoluted by two components, originating from the excitation of the polymer and $PC_{71}BM$ domains respectively: (i) a fast decay of the polymer excitons, which is especially visible for the coarse blend prepared without additives and (ii) a slow signal increase as $PC_{71}BM$ excitons diffuse to the interface and are separated into charge pairs which causes an increase of the polymer GSB.

The first component is largely identical to the kinetics measured by exciting only the polymer domains at λ_{exc}=800 nm (Figure 7). The kinetics of the second component can therefore be isolated by subtraction of the λ_{exc}=800 nm kinetics for the same blends. The scaling factor of the subtracted kinetics was determined by comparison of the excitation fluences in the two TA measurements and the absorption of the polymer domains at 530 nm and 800 nm. The isolated kinetics of the second component are shown in Figure 8 (b).

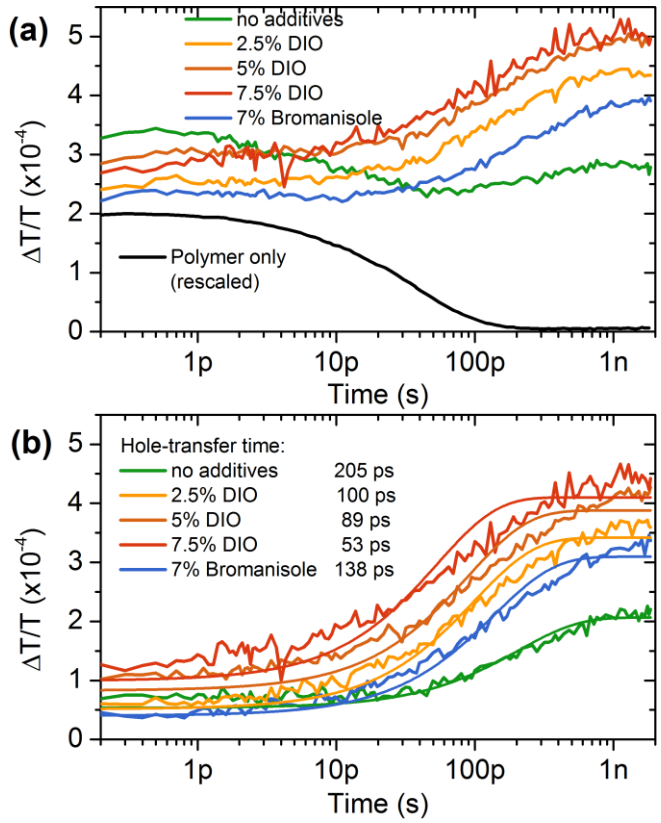

Figure 8 a) TA kinetics at the polymer GSB position (averaged over 750-820 nm) under excitation at 530 nm. The decay of the polymer only film (excited at 800 nm) is shown for comparison. Figure (b) shows the same kinetics after subtraction of the rescaled decay kinetics with excitation at 800 nm.

The hereby obtained kinetics were fitted with single exponential functions $A + (1-y_0 \cdot e^{t/\tau 1})$ in order to extract the timescales and yield for the diffusion-limited hole-transfer from the $PC_{71}BM$ to the polymer. These corrected kinetics show that only a small fraction of charges are formed ultrafast (<1 ps) and that the majority of charge formation happens over the time-scale of tens of ps to 2 ns. The data further shows a faster charge formation rate and a higher charge formation yield for the blends with finer morphology, prepared with DIO. We attribute the faster and more efficient charge transfer to the shorter diffusion length required for the $PC_{71}BM$ excitons to reach the polymer-$PC_{71}BM$ interface. We note that the GSB kinetics in Figure 8 (b) show a signal rise up to ~2 ns, which is longer than the $PC_{71}BM$ singlet exciton lifetime of ~770 ps.[33] This surprisingly slow hole-transfer suggests that the charge formation is mainly limited by the exciton diffusion to the interface. It is likely that an even finer morphology would further increase the charge formation but possibly at the detriment of charge percolation pathways. Unlike in the measurements with λ_{exc}=800 nm, the charge formation yield and rate seem to steadily increase with higher concentrations of DIO. This would imply that the $PC_{71}BM$ domain sizes further decrease with higher concentrations of DIO.

A more quantitative approach can be used to estimate the charge formation yield in the TA measurements. In a first step, the absorption cross-section of the polymer exciton is calculated from the measurements at λ_{exc}=800 nm: Based on the GSB signal intensity of $3*10^{-4}$ at the peak position of the GSB (700-800 nm), the employed excitation fluence (2.5 μJcm^{-2} at λ_{exc}=800 nm) and the absorption of the film, a GSB cross-section of $4.6*10^{-17}$ cm^{-2} at 800 nm is obtained. In the TA kinetics of the hole-transfer from $PC_{71}BM$ to the polymer in Figure 8 a) the GSB signals rise to $\sim 4.5 \cdot 10^{-4}$ at 2 ns for the blends prepared with DIO. A comparison with the polymer exciton GSB cross-section, as well as the excitation fluence (15 μJcm at λ_{exc}=530 nm) and the film absorption at this wavelength suggests that this signal only corresponds to ~24% of the initial excitations. This would imply that 75% of the initial excitations in the $PC_{71}BM$ domains do not end up in longer-lived charges. We note that this calculation assumes equal GSB cross-sections for the DPP-polymer excitons and a charge pair with a positive charge on the polymer. If the GSB of a charge pair would only have half the strength of an exciton, then the long-lived GSB would represent ~48% of initial excitations, rather than the ~24%. The low yield of charge formation is comparable with IQE values obtained for the devices prepared with DIO. This suggests that the majority of charges formed can also be extracted and that the device performance is mainly limited by the charge formation and not by charge extraction from the device.

We note, however, that the charge formation efficiency of < 50% calculated here is below the 75-80% photoluminescence quenching obtained for the blends with excitation of the $PC_{71}BM$ domains (Figure 5). This discrepancy is likely caused by impure $PC_{71}BM$ domains which lead to efficient exciton quenching and short-lived CT-states, rather than free charges which can diffuse away from the BHJ interface. A similar explanation has been proposed in the previous discussion of the TA measurements with excitation of the polymer domains at 800 nm.

Long-time TA Measurements

While the short-time TA measurements up to 2 ns provide useful information about the charge formation processes, they do not cover the ns-μs time-range over which charges are extracted from the device. In order to probe the dependence of the free charge recombination dynamics on the charge density, nanosecond to microsecond TA measurements were carried out at different excitation fluences. Figure 9 a) shows the TA kinetics averaged over the polymer GSB region (750-850 nm) after excitation at 532 nm for blends prepared with DIO and without solvent additives. To better visualize the two recombination regimes the kinetics were normalized at 500 ns after excitation. The first decay regime shows a strong excitation fluence dependence, with a faster and more pronounced decay at high fluence. These fluence dependent decay kinetics are a common observation for measurements at high initial excitation densities and we assign them to the geminate recombination of free charges in agreement with previous literature.[38, 39] The non-geminate recombination of free charges continues until about 500 ns, when a charge density level is reached at which non-geminate recombination become less significant. From about 500 ns onwards the recombination kinetics were found to be independent of the initial excitation intensity and blend morphology. Previous studies by other groups have assigned a slower, intensity independent decay on the same time-scale to bimolecular recombination of charges in the presence of an exponential tail of trap sites. In these studies the trap-assisted recombination was found to follow power-law decays ($\Delta T/T \propto t^{-\alpha}$) with exponents in the range of 0.4-0.5.[39] A power-law fit of our data

up to a delay time of 20 µs returned an exponent of only α=0.14, much lower than previous values for trap-assisted recombination. We therefore argue that the slower recombination regime is merely a continued recombination of free charge carriers, which have escaped the interface after the charge carrier density has dropped to a level below which the morphology can support.

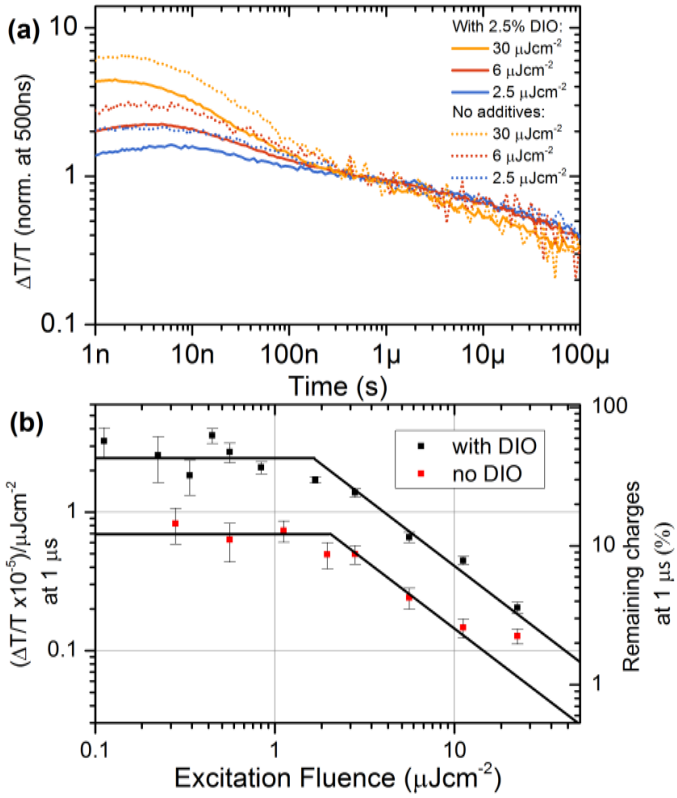

Figure 9: a) Nanosecond TA kinetics of the GSB recovery averaged over 750-850 nm and normalized to 1 at a delay time of 500 ns under 532 nm excitation. b) Charge yield measured as the GSB intensity at 800 nm at 1 µs after excitation plotted over the excitation fluence for films prepared with and without the solvent additive DIO. The flat trend-line at low fluence represents the regime where no non-geminate recombination occurs over the first 1 µs. The inverse power-law trend-lines at high fluence represent the regime, where the charge density at 1 µs is independent of excitation fluence caused by fast non-geminate recombination of charge carriers up to the maximum carrier density which the blend can support.

To illustrate the threshold for the non-geminate recombination of free charges, the GSB signal intensity at 1µs per excitation fluence is plotted over the excitation fluence in Figure 9 (b). In the linear regime up to excitation fluences of ~2 µJcm^{-2} the charge density is below the threshold of excitation-fluence dependent non-geminate recombination. Above ~2 µJcm^{-2} the charge density at 1 µs is independent of the initial excitation fluence, indicated by the trend-lines with inverse power-law. The right-hand axis indicates the charge density at 1µs as a fraction of the initial number of photoexcitations. These values were calculated based on the GSB cross-section of 4.6*10^{-17} cm^{-2} at 700-800 nm as discussed earlier.

The two blends show similar excitation fluence dependences. However, the total charge density at any given fluence is about three times higher for the blend with the finer morphology, prepared with DIO. This suggests that the finer morphology allows the blend to support a higher density of charges before fast non-geminate recombination occurs. This is another indication that the increased device performance is caused by the improved morphology and not by a modification of the interface.

Discussion:

The short exciton lifetime has direct consequences for the efficiency of exciton diffusion and charge separation. Exciton diffusion in conjugated polymers takes place by two separate processes, short-range electron tunnelling processes and Förster type resonant energy transfer (FRET).[5, 6, 40] The latter mechanism requires a spectral overlap between the donor molecule emission spectrum and the acceptor molecule absorption spectrum. The strength of this transfer integral and thus the FRET efficiency depend on the energy landscape inside the polymer domains as well as on the fluorescence efficiency of the polymer.[5] The exciton diffusion length increases with the square root of the exciton lifetime which is therefore an important parameter for efficient exciton dissociation.[4] According to the energy gap law, the non-radiative decay rate by multi-phonon processes increases exponentially with a reduction of the band-gap.[7-9] As a direct consequence of its low band-gap, the decay of the DPP-polymer singlet excitons is significantly faster than the exciton lifetime of higher band-gap, high performance OPV polymers. Based on the singlet exciton lifetime of 35 ps and the photoluminescence quantum efficiency of 0.06% we obtain radiative and non-radiative decay rate of 1.7*10^{7} s^{-1} and 2.9*10^{10} s^{-1} respectively.[41] The radiative decay rate is in the same range as that of rr-P3HT (5*10^{7} s^{-1}), whereas the non-radiative decay rate is almost by a factor of 20 higher than that of rr-P3HT at 1.6*10^{9} s^{-1}.[42] The comparatively low radiative decay rate of the DPP-polymer suggest that the exciton also reaches a state with weak radiative coupling to the ground state, similar to the H-aggregate states in rr-P3HT.[43] The comparison between the DPP-polymer and P3HT shows that the single most important reason for the short exciton diffusion length is the high non-radiative decay rate in the low band-gap polymer. We note that this is not specific to the material studied here, but rather represents a general trend with low band-gap polymers. Unless the shorter exciton lifetime can be compensated by higher exciton diffusion by short-range tunnelling processes, the exciton diffusion length will be reduced, possibly below the common range of 5-10 nm of most emissive conjugated polymers.[1] The shorter exciton diffusion length of low band-gap polymers which arises from the short exciton lifetimes could have wide-ranging ramifications for the design of low band-gap OPV systems. As the exciton diffusion length shortens, only excitons very close to the $PC_{71}BM$ domain interface can dissociate efficiently into charge-pairs. The trend towards lower band-gaps will therefore require finer donor-acceptor morphologies to maintain the same charge separation efficiencies. On the other side, finer morphologies generally reduce the efficiency of charge extraction from the device. The trend towards low band-gap polymers will therefore make it more critical and more challenging to optimise the bulk heterojunction morphology.

We consider that the exciton lifetime and associated exciton diffusion length are important parameters which impact the efficiency of OPV devices. Most existing models only consider energetic parameters, which might be one reason why OPV performances are often very unpredictable for new materials.[44]

Conclusions

We quantitatively analysed the device performance, excited state dynamics and loss mechanisms in DPP-polymer:$PC_{71}BM$ solar cells, prepared either with and without the high boiling point solvent additive DIO. The solvent additive was identified to act as compatibilizer between the two materials and hence prevents large-scale phase separation and increases device efficiency. The finer BHJ morphology was found to increase the fraction of polymer excitons which travel to the donor-acceptor interface and are separated into free charges. However, even in the improved devices with a much finer morphology, less than 50% of polymer excitons reach this interface. The very short polymer exciton lifetime, as a consequence of the low band-gap and the energy gap law, has been identified as one of the reasons for the incomplete exciton quenching. A significant fraction of the polymer excitons which are separated at the donor-acceptor interface were found to geminately recombine, constituting a significant loss channel of around one quarter of all photoexcited states. As a consequence of the low conversion efficiency of polymer excitons into free charges, the polymer is outperformed by the $PC_{71}BM$, which is responsible for almost 2/3 of the generated photocurrent. We have identified the much longer $PC_{71}BM$ exciton lifetime as one of the reasons for its strong contribution to the photocurrent.
Further, we have shown that the intrinsic short lifetime of low band-gap polymer poses an obstacle towards further improvements of the device efficiency. Development of polymers with even lower band-gap should therefore include other approaches, such as ways to increase the exciton diffusion rate or in the design of optimized morphologies with smaller feature sizes.

Acknowledgements

The authors acknowledge financial support from the EPSRC, UK and the Department of Science and Technology, India through the Indo-UK APEX Program. D.-H. Ko also acknowledges support from grants 2E23892 and 2E23650 from KIST. The authors thank Akshay Rao for useful discussion and Alessandro Sepe for the help with the X-ray measurements. These measurments were carried out at beamline I22 at the Diamond Light Source, Harwell UK.

References

1. S. R. Scully and M. D. McGehee, *J. Appl. Phys.*, 2006, **100**, 034907-034905.
2. G. Yu, J. Gao, J. C. Hummelen, F. Wudl and A. J. Heeger, *Science*, 1995, **270**, 1789-1791.
3. J. J. M. Halls, C. A. Walsh, N. C. Greenham, E. A. Marseglia, R. H. Friend, S. C. Moratti and A. B. Holmes, *Nature*, 1995, **376**, 498-500.
4. P. E. Shaw, A. Ruseckas and I. D. W. Samuel, *Adv. Mater.*, 2008, **20**, 3516-3520.
5. M. A. Stevens, C. Silva, D. M. Russell and R. H. Friend, *Phys. Rev. B*, 2001, **63**, 165213.
6. J. M. Hodgkiss, S. Albert-Seifried, A. Rao, A. J. Barker, A. R. Campbell, R. A. Marsh and R. H. Friend, *Adv. Funct. Mater.*, 2012, **22**, 1567-1577.
7. J. S. Wilson, N. Chawdhury, M. R. A. Al-Mandhary, M. Younus, M. S. Khan, P. R. Raithby, A. Köhler and R. H. Friend, *J. Am. Chem. Soc.*, 2001, **123**, 9412-9417.
8. M. Pope and E. S. Charles, *Electronic Processes in Organic Crystals and Polymers*, Oxford University Press, New York, Oxford, 1999.
9. R. Englman and J. Jortner, *Mol. Phys.*, 1970, **18**, 145-164.
10. J. Peet, C. Soci, R. C. Coffin, T. Q. Nguyen, A. Mikhailovsky, D. Moses and G. C. Bazan, *Appl. Phys. Lett.*, 2006, **89**, 252105.
11. A. R. Campbell, J. M. Hodgkiss, S. Westenhoff, I. A. Howard, R. A. Marsh, C. R. McNeill, R. H. Friend and N. C. Greenham, *Nano Lett.*, 2008, **8**, 3942-3947.
12. J. Peet, J.-S. Kim, N. E. Coates, W. L. Ma, D. Moses, A. J. Heeger and G. C. Bazan, *Nature Materials*, 2007, **6**, 497-500.
13. F. Etzold, I. A. Howard, N. Forler, D. M. Cho, M. Meister, H. Mangold, J. Shu, M. R. Hansen, K. Müllen and F. Laquai, *J. Am. Chem. Soc.*, 2012, **134**, 10569-10583.
14. I.-W. Hwang, S. Cho, J. Y. Kim, K. Lee, N. E. Coates, D. Moses and A. J. Heeger, *J. Appl. Phys.*, 2008, **104**, 033706-033709.
15. D. Di Nuzzo, A. Aguirre, M. Shahid, V. S. Gevaerts, S. C. J. Meskers and R. A. J. Janssen, *Adv. Mater.*, 2010, **22**, 4321-4324.
16. J. K. Lee, W. L. Ma, C. J. Brabec, J. Yuen, J. S. Moon, J. Y. Kim, K. Lee, G. C. Bazan and A. J. Heeger, *J. Am. Chem. Soc.*, 2008, **130**, 3619-3623.
17. J. W. Jung, F. Liu, T. P. Russell and W. H. Jo, *Energy & Environmental Science*, 2012, **5**, 6857-6861.
18. S. J. Lou, J. M. Szarko, T. Xu, L. Yu, T. J. Marks and L. X. Chen, *J. Am. Chem. Soc.*, 2011, **133**, 20661-20663.
19. M.-S. Su, C.-Y. Kuo, M.-C. Yuan, U. S. Jeng, C.-J. Su and K.-H. Wei, *Adv. Mater.*, 2011, **23**, 3315-3319.
20. J. K. Park, C. Kim, B. Walker, T.-Q. Nguyen and J. H. Seo, *RSC Advances*, 2012, **2**, 2232-2234.
21. X. Liu, S. Huettner, Z. Rong, M. Sommer and R. H. Friend, *Adv. Mater.*, 2012, **24**, 669-674.
22. W. Li, W. S. C. Roelofs, M. M. Wienk and R. A. J. Janssen, *J. Am. Chem. Soc.*, 2012.
23. L. Dou, J. You, J. Yang, C.-C. Chen, Y. He, S. Murase, T. Moriarty, K. Emery, G. Li and Y. Yang, *Nat Photon*, 2012, **6**, 180-185.
24. A. T. Yiu, P. M. Beaujuge, O. P. Lee, C. H. Woo, M. F. Toney and J. M. J. Fréchet, *J. Am. Chem. Soc.*, 2011, **134**, 2180-2185.
25. T. J. K. Brenner, Z. Li and C. R. McNeill, *The Journal of Physical Chemistry C*, 2011, **115**, 22075-22083.
26. B. Friedel, B. Ehrler, S. Hüttner and N. C. Greenham, *Small*, 2012, **8**, 237-240.
27. C. V. Hoven, X.-D. Dang, R. C. Coffin, J. Peet, T.-Q. Nguyen and G. C. Bazan, *Adv. Mater.*, 2010, **22**, E63-E66.
28. P. Kohn, Z. Rong, K. H. Scherer, A. Sepe, M. Sommer, P. Müller-Buschbaum, R. H. Friend, U. Steiner and S. Hüttner, *Macromolecules*, 2013.
29. J. C. de Mello, H. Felix Witttmann and R. H. Friend, *Adv. Mater.*, 1997, **9**, 230-232.
30. S. Cook, A. Furube, R. Katoh and L. Han, *Chem. Phys. Lett.*, 2009, **478**, 33-36.
31. J. R. Moore, S. Albert-Seifried, A. Rao, S. Massip, B. Watts, D. J. Morgan, R. H. Friend, C. R. McNeill and H. Sirringhaus, *Advanced Energy Materials*, 2011, **1**, 230-240.
32. G. Cirmi, D. Brida, C. Manzoni, M. Marangoni, S. De Silvestri and G. Cerullo, *Opt. Lett.*, 2007, **32**, 2396-2398.
33. P. Chow, S. Albert-Seifried, S. Gélinas and R. H. Friend, in preparation.

34. R. A. Marsh, J. M. Hodgkiss, S. Albert-Seifried and R. H. Friend, *Nano Lett.*, 2010, **10**, 923-930.
35. S. Albert-Seifried and R. H. Friend, *Appl. Phys. Lett.*, 2011, **98**, 223304.
36. A. A. Bakulin, A. Rao, V. G. Pavelyev, P. H. M. van Loosdrecht, M. S. Pshenichnikov, D. Niedzialek, J. Cornil, D. Beljonne and R. H. Friend, *Science*, 2012, **335**, 1340-1344.
37. T. W. Holcombe, J. E. Norton, J. Rivnay, C. H. Woo, L. Goris, C. Piliego, G. Griffini, A. Sellinger, J.-L. Brédas, A. Salleo and J. M. J. Fréchet, *J. Am. Chem. Soc.*, 2011, **133**, 12106-12114.
38. J. Nelson, *Phys. Rev. B*, 2003, **67**, 155209.
39. T. Clarke, A. Ballantyne, F. Jamieson, C. Brabec, J. Nelson and J. Durrant, *Chem. Commun.*, 2009, 89-91.
40. S. M. King, D. Dai, C. Rothe and A. P. Monkman, *Phys. Rev. B*, 2007, **76**, 085204.
41. *Based on the formula for the photoluminescence quantum efficiency: $PLQE=k_r/(k_r+k_{nr})$.*
42. *Based on the molecular fluorescence lifetime of 600ps and a PLQE of 3% which are average values reported in the literature.*
43. J. Clark, C. Silva, R. H. Friend and F. C. Spano, *Phys. Rev. Lett.*, 2007, **98**, 206406.
44. D. Credgington and J. R. Durrant, *The Journal of Physical Chemistry Letters*, 2012, **3**, 1465-1478.

